coatings

MDPI

Article

Physical and Chemical Properties of High-Temperature Silicone-Based Polymer Coatings Applied on Different Surface Roughnesses

Ivan Stojanović *, Borna Škrlec, Marin Kurtela, Vesna Alar and Martina Odeljan

Faculty of Mechanical Engineering and Naval Architecture, University of Zagreb, 10000 Zagreb, Croatia; borna.skrlec@fsb.unizg.hr (B.Š.); marin.kurtela@fsb.unizg.hr (M.K.); vesna.alar@fsb.unizg.hr (V.A.); martina.odeljan@fsb.unizg.hr (M.O.)

* Correspondence: ivan.stojanovic@fsb.unizg.hr

Abstract: High-temperature coatings play a crucial role in protecting surfaces exposed to extreme temperatures, corrosion, and other harsh environments. This paper focuses on the physical and chemical properties of solvent-borne and water-borne high-temperature silicone-based polymer coatings applied on two types of surface roughness of carbon steel plates. The corrosion protection performance of the coatings was characterized using a salt spray chamber, humidity chamber, electrochemical impedance spectroscopy (EIS) measurements, and differential scanning calorimetry (DSC). The physical properties of high-temperature coatings were determined using the Shore D hardness method and cross-cut adhesion tests. This study investigates the effects of different surface preparation methods on coating adhesion, which is considered to be a crucial property of organic coatings for corrosion protection durability. The thermal stability of the coating was tested using furnace cyclic testing. The results show that high-temperature coatings in general exhibit excellent thermal stability, high adhesion strength, and good resistance to warm and humid environments, except in the conditions of a salty atmosphere. This study reveals that coating performance is affected by the composition and surface preparation method. This study can be useful for coating manufacturers and researchers interested in understanding the physical and chemical properties of high-temperature coatings and their applications in various environments.

Keywords: corrosion; high-temperature coatings; physical properties; chemical properties

check for updates

Citation: Stojanović, I.; Škrlec, B.; Kurtela, M.; Alar, V.; Odeljan, M. Physical and Chemical Properties of High-Temperature Silicone-Based Polymer Coatings Applied on Different Surface Roughnesses. *Coatings* **2023**, *13*, 2100. https://doi.org/10.3390/coatings13122100

Academic Editor: Albano Cavaleiro

Received: 24 November 2023
Revised: 12 December 2023
Accepted: 17 December 2023
Published: 18 December 2023

Copyright: © 2023 by the authors. Licensee MDPI, Basel, Switzerland. This article is an open access article distributed under the terms and conditions of the Creative Commons Attribution (CC BY) license (https://creativecommons.org/licenses/by/4.0/).

1. Introduction

Corrosion protection significantly affects the functionality of a structure, its durability, and operational safety, thereby playing a substantial role in construction and maintenance. Coating protection is the most widely used method for safeguarding various steel structures against corrosion. In the technology of coating protection, it is crucial to correctly execute all technological operations involving surface preparation and coating application. Alongside quality, protective processes are increasingly needed to meet environmental and human non-harmfulness requirements.

High temperature is a critical factor influencing the occurrence and development of corrosion, greatly reducing the product or machinery component's lifespan. High-temperature corrosion is a type of corrosion that emerges where temperatures are well above 100 °C, such as in chimney flues, automobile exhaust systems, diesel engines, power plants, gas turbines, and other machinery in contact with hot gases containing certain impurities [1,2]. For higher temperatures up to 900 °C, the most commonly used materials are aluminum oxide and chromium (III) oxide, while silicon dioxide can withstand temperatures up to 1800 °C [3]. These oxide films represent a special type of coating that creates an oxide protective layer between the high-temperature oxidative environment and the material itself. For this oxide layer to fulfill its material protection purpose, it needs

to remain stable at high temperatures, adhere well to the material's substrate, possess a certain density, and be resistant to the thermal shock caused by rapid temperature changes.

Among corrosion protection methods, organic coating protection stands out due to its effectiveness, which depends on various factors like environmental corrosiveness, the type of protected surface, coating system durability, surface preparation, and the coating application technology. Materials employed in high-temperature environments must meet specific criteria like mechanical or thermodynamic fatigue strength, while the coating itself must provide suitable environmental resistance and be chemically and mechanically compatible with the substrate [4]. High-temperature paint must withstand high temperatures without decomposing, cracking, or delaminating [5]. The purpose of these high-temperature protective coatings and paints is to maintain external appearance and heat resistance over extended periods at high temperatures [6]. The thermal stability limit of commonly available coating systems is typically around 60 °C [7]. Epoxy systems using conventional bisphenol-A-based resin are generally limited to a service temperature of around 80–90 °C [8]. At temperatures ranging from 200 °C to 300 °C, most organic-based coatings undergo carbonization, and in some cases, this carbonization is accompanied by the development of aggressive gases such as hydrogen chloride from PVC [9]. Coatings for wood-burning fireplaces must endure temperatures up to 600 °C. For such applications, coatings based on silicone resins are widely used due to their excellent high-temperature resistance [3]. Compared with homologous carbon-based polymers, silicone resins show superior performance in thermal stability due to the physicochemical properties of the siloxane (-Si-O-Si) bond [10]. In high-temperature applications, solvent- and water-based inorganic zinc-rich silicate coatings are also used [11].

A coating protection study is a complex and comprehensive issue that requires a lot of experimental work to obtain the proper physical and chemical properties of the coatings. Authors [12,13] used electrochemical impedance spectroscopy (EIS) as a method to evaluate the condition of the coating surface and its barrier properties, which are key to achieving satisfactory corrosion resistance of the coating. Chen et al. [14] used a neutral salt spray test to accelerate the indoor aging of cold-spray aluminum zinc, hot-spray zinc, and hot-dip zinc coatings. After the salt spray test adhesion was determined by the method of a scratch test. Tsai et al. [15] evaluated high-performance polyurethane/graphene composite coatings using various corrosion and mechanical tests, namely electrochemical impedance spectroscopy, salt spray tests, cross-cut tape tests, and dynamic mechanical analysis. The cross-cut test is a standard test method for the adhesion of organic coatings. The grade of adhesion quality in the cross-cut test is rated from 0 to 5; 0 and 5 represent the best and poorest adhesion performances, respectively [16]. The humidity test for paint helps assess coating quality in 100% relative humid conditions and elevated temperatures. Aračić et al. [17] performed research on the new generation of paint systems for the anticorrosion protection of steel structures using a humidity chamber. Panels were placed inside a humidity chamber and exposed continually for a specified period according to ISO 6270 [18], then evaluated for degradation according to ISO 4628 [19]. The standard ISO 4628 refers to the designation of quantity and size of defects and of intensity of uniform changes in appearance, namely blistering, rusting, cracking, flaking, chalking, delamination, and degree of filiform corrosion. The testing in the water vapor atmosphere served to determine the behavior of the material exposed to the moisture-saturated warm air in the presence of condensed water.

Previous studies on silicone-based coatings included the type of silicone resin for the long-term heat resistance of the coating [3], adhesion properties, variety of precursors and polymer-to-ceramic conversion of silicone-based coatings [20], chemical properties of silane-based coatings [21], flake ZnAl alloy as an effective pigment in silicate coatings for the corrosion protection of steel [22], and the interface properties between water-based inorganic zinc silicate coating modified by organosilicon and iron substrate [11].

To our knowledge, a detailed comparison of physical and chemical properties between the water-borne and solvent-borne silicone-based polymer coatings applied on different

surface roughnesses has not been extensively reported. The evaluation of their resilience against varied environmental conditions and thermal stress in this work provides a different approach to a critical aspect that has remained insufficiently unexplored in the existing research literature.

This study aims to investigate the physical and chemical properties of two solvent-borne compared to two water-borne high-temperature coatings used for the protection of wood-burning fireplaces using a salt spray chamber, humidity chamber, cyclic low–high temperature exposure, electrochemical impedance testing (EIS), and differential scanning calorimetry (DSC). Special attention is given to the examination of the influence of surface roughness and profile on the adhesion of coatings. The corrosion properties and thermal stability of commercially available water-based high-temperature paints were evaluated to assess their suitability for prospective applications and to provide researchers with reference data compared to traditionally used solvent-based paints. Based on these tests, the properties and appearance of coatings that align with the real-use application conditions for wood-burning stoves will be defined.

2. Materials and Methods

2.1. Materials

The metallic substrate used for this study was EN 10111 DD13 low-carbon hot-rolled steel with the chemical composition 0.04 C, 0.20 Mn, 0.008 P, 0.05 S, and Fe in balance (wt.%). The material is used for stove manufacturing. The dimension of the sample was 100 × 150 × 3 mm, and the surface of the samples was prepared by abrasive blasting in two ways: half of the samples were sandblasted (letter P in the sample designation), and the other half of the samples were shot-blasted (letter S in the sample designation). The surface roughness was measured using a TMR200 surface roughness gauge (TMTeck Instrument Co., LTD., Beijing, China).

2.2. Preparation of the Coatings

The study was conducted on the four types of high-temperature silicone-based polymer coatings, two of which are solvent-based (Solvalitt Black, Resist 78), and the other two coatings (Senotherm UHT 2K-Hydro 3590, Thermodur 600 Aqua) are new water-based high-temperature formulations. Their characteristics are presented in Table 1. The described coatings were prepared, applied, and dried in room condition according to the manufacturer's instructions.

Table 1. Properties of the tested coatings.

Coating	Label	Base	Temperature Resistance, °C	Density kg/L	Wet Film Thickness, µm	Dry Film Thickness, µm	Volume Sold, %	Theoretical Spreading Rate
Solvalitt Black	SO	Silicone acrylic coating	600	1.30	50–70	20–30	43 ± 2	21–14 m^2/L
Thermodur 600 Aqua	TH	Water-based modified silicone resin	600	1.29	53–107	15–30	28	11 m^2/kg
Senotherm UHT 2K-Hydro 3590	SE	Water-based	600	-	47	25	53	9 m^2/kg
Resist 78	RE	Inorganic zinc ethyl silicate	540	2.50	70–125	50–90	72 ± 2	14.4–8 m^2/L

The preparation of samples is visually represented in the schematic diagram in Figure 1.

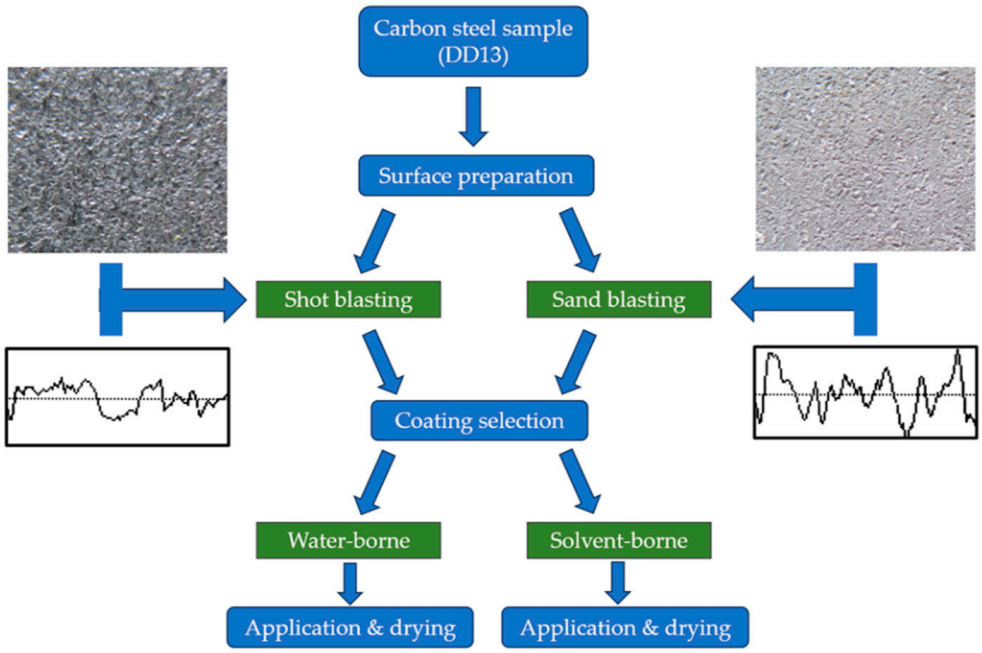


Figure 1. Flow diagram of the procedures for the preparation of the samples used in this research.

2.3. Dry Film Thickness, Adhesion, and Gloss

After the coating application, the coating thickness was determined using an Elcometer 456 device (Elcometer Limited, EdgeLane, Manchester, UK), according to ISO 2808 [23]. Measurements were made at 10 different places per sample with instrument accuracy of ±2.5 µm, and the mean value was calculated. Adhesion was tested using the "Cross-cut" method and a Zehntner ZCT 2160.123 G device (Zehntner GmbH Testing Instruments, Sissach, Switzerland), according to ISO 2409 [16]. Also, hardness testing was conducted using the Shore D method and a PosiTector SHD durometer (DeFelsko Corporation, NY, USA) with an accuracy of ±1.

2.4. Accelerated Testing in Chambers

One set of samples was tested in a salt spray chamber, the second in a humidity chamber, and the third was tested for temperature cycle endurance, with a maximum achieved temperature of 450 °C. After the accelerated testing in chambers, the coatings were evaluated according to ISO 4628.

Regarding the salt spray chamber, the samples were tested in the Ascott S450 salt spray chamber (Ascott Analytical Equipment Limited, Staffordshire, UK), according to ISO 9227 [24], with the parameters provided in Table 2. The samples were subjected to corrosion conditions in a salt atmosphere for 96 h, i.e., four days.

Table 2. Testing parameters in the salt chamber.

Testing Parameters	Standard	Testing Conditions
Testing Duration, hours	As agreed	96
Temperature, °C	35 ± 2	35 ± 0.1
Testing Chamber Volume, liters	min 400	450
Air Humidifier Temperature, °C	45–50	47
Compressed Air Pressure, bar	0.7–1.4	0.98
Used Solution	NaCl	NaCl
Solution Concentration, %	5	5
Collected Condensate Amount, mL/80 cm^2/h	1.5 ± 0.5	2.0
Condensate pH Value at 25 ± 2 °C	6.5–7.2	7.1
Conductivity of Distilled Water, µS/cm at 25 ± 2 °C	max 20	<10

On the samples that were in the salt spray chamber, a scribe was made to assess the corrosion under the coating. According to ISO 12944-6 [25], corrosion around the scribe should not exceed 1.5 mm, calculated as:

$$M = (C - W)/2 \quad (1)$$

where C is the maximum width of corrosion across the scratch, and W is the original width of the scribe in millimeters.

As for the humidity chamber, it simulates conditions of a warm and humid atmosphere with water condensation. The testing in the humidity chamber was conducted in the Humidity Cabinet Model AB6 (C&W Specialist Equipment, Belrose, NSW, Australia), following the ISO 6270-2 standard [18]. The testing temperature was 40 °C, and the relative humidity in the chamber was approximately 100%, resulting in the samples experiencing condensation.

The furnace cyclic testing was carried out as part of the coating adhesion and appearance validation after cyclic exposure to low/high temperature environments.

Views of the samples at the beginning of testing in the salt spray chamber and humidity chamber are provided in Figure 2.

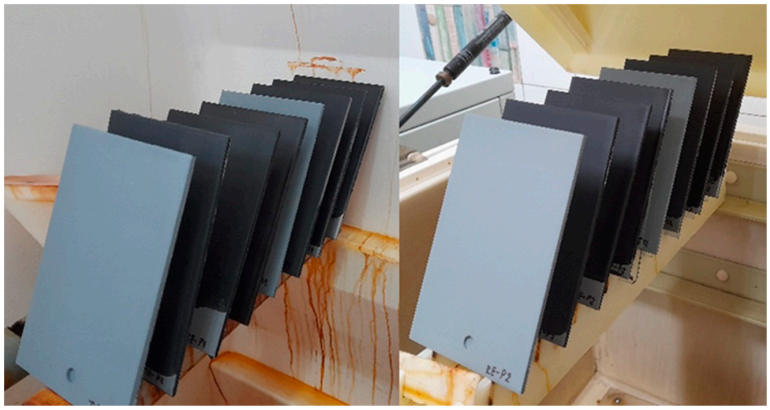


Figure 2. Samples ready for testing in the salt spray chamber (**left**) and humidity chamber (**right**).

2.5. Electrochemical Characterization

Electrochemical characterizations of the coatings were performed by measuring the electrochemical impedance spectroscopy (EIS). Electrochemical impedance spectroscopy has a key role in understanding electrochemical behavior at the metal/coating interface and determining the resistance properties of a coating [12]. The application of EIS enabled the quantification of the surface layer resistance and the definition of the mechanism of corrosion progression without any degradation of the test surface. EIS was conducted using a VersaSTAT 3 Potentiostat/Galvanostat (AMETEK Scientific 131 Instruments, Princeton applied research, Berwyn, PA, USA), with the application of ZsimpWin 3.60 software. The tested electrochemical cell consisted of a metal substrate with a coating as a working electrode, a saturated calomel electrode as a reference electrode, and two graphite rods as counter electrodes. The coating properties were determined in a 3.5 wt.% NaCl solution, at a frequency range of 0.1 to 10^5 Hz and at room temperature (23 ± 2 °C).

2.6. Differential Scanning Calorimetry (DSC)

A Mettler Toledo differential scanning calorimeter DSC 3+ (Mettler Toledo, Greifensee, Switzerland) was used to carry out the differential thermal analysis and determine the glass transition temperature (T_g). Samples of 10 mg were analyzed in a stream of nitrogen (40 mL/min) with a heating and cooling rate of 10 °C/min in a temperature range from −100 °C to 150 °C by a double heating/cooling cycle. Samples were first heated from 25 °C to 150 °C at a rate of 10 °C/min and held at that temperature for 5 min to erase the

thermal history of the sample during the preparation process. Samples were then cooled from 150 °C to −100 °C at a cooling rate of 10 °C/min, held at −100 °C for 5 min, and reheated from −100 °C to 150 °C at a rate of 10 °C/min [13]. Liquid nitrogen was used to cool the samples to low temperatures. From the second heating cycle, values of the glass transition temperature T_g were obtained. The glass transition temperature represents the temperature at which an amorphous polymer changes from a rigid, glassy state to a more flexible, rubbery state. Knowing the T_g of coatings is crucial, as it provides valuable insights into the material's mechanical and thermal properties and helps to define the appropriate temperature range for the application and utilization of the coating.

Methods and procedures for the evaluation of coating stability are visually represented in the diagram in Figure 3.

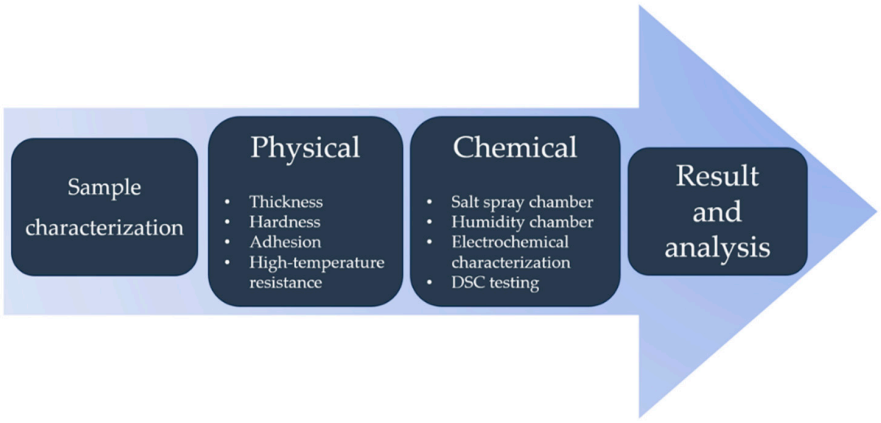


Figure 3. Flow diagram of the methods for the evaluation of coating stability.

3. Results and Discussion

3.1. Surface Roughness, Coating Thickness, and Hardness Testing

The average surface roughness value on sandblasted samples was 23.58 µm with irregular sharp surfaces, while on shot-blasted ones, it was 18.65 µm with rounded profiles. The substrates on both sample groups were prepared to the required cleanliness of Sa 2.5, according to ISO 8501-1 [26].

After coating the steel plates, the coating thickness was measured. Thickness was measured at 10 different points on each sample, and the average value is recorded in Tables 3 and 4. The lowest coating thickness was observed on water-based modified silicone resin TH: from 10.3 µm to 11.3 µm. The measurement of coating thickness revealed that inorganic zinc ethyl silicate RE has the greatest thickness, from 27.6 µm to 33.9 µm.

Table 3. Coating thickness, hardness, and adhesion on sandblasted samples.

Sandblasted Samples				
Sample	$\bar{x}$ **(µm)**	**Shore D Hardness**	**Cross-Cut**	**Test Type**
SO-P1	21.2	93.6		Salt chamber
SO-P2	22.0	92.6		Humidity chamber
SO-P3	15.9	93.2	0	Cyclic temperature
SE-P1	14.4	93.8		Salt chamber
SE-P2	15.3	94.6		Humidity chamber
SE-P3	17.1	94.2	0	Cyclic temperature
TH-P1	10.9	91.6		Salt chamber
TH-P2	11.1	93.6		Humidity chamber
TH-P3	11.3	92.4	0	Cyclic temperature
RE-P1	33.9	93.8		Salt chamber
RE-P2	31.4	93.6		Humidity chamber
RE-P3	31.2	93.1	0	Cyclic temperature

Table 4. Coating thickness, hardness, and adhesion on shot-blasted samples.

Shot-Blasted Samples				
Sample	$\bar{x}$ **(µm)**	**Shore D Hardness**	**Cross-Cut**	**Test Type**
SO-S1	26.7	93.6		Salt chamber
SO-S2	24.0	92.4		Humidity chamber
SO-S3	20.3	93.3	1	Cyclic temperature
SE-S1	17.1	93.6		Salt chamber
SE-S2	12.0	94.6		Humidity chamber
SE-S3	13.3	93.2	1	Cyclic temperature
TH-S1	10.3	92.0		Salt chamber
TH-S2	11.2	93.8		Humidity chamber
TH-S3	10.3	92.1	0	Cyclic temperature
RE-S1	27.6	93.8		Salt chamber
RE-S2	33.8	93.8		Humidity chamber
RE-S3	27.8	93.6	1	Cyclic temperature

The coating hardness testing was conducted by the Shore D method. Ten measurements were taken on each sample, and the average value is recorded in Tables 3 and 4. It is evident that the results are similar, indicating that hardness is independent of the type of tested coating but mostly influenced by the steel substrate. Coating hardness testing was carried out to assess resistance to abrasion, which is a crucial property indicating the integrity of the coating during use. A low coating hardness makes it susceptible to damage [27].

3.2. Coating Adhesion Testing

Tables 5 and 6 present the results of adhesion testing by the cross-cut method, according to the ISO 2409 standard, on samples after accelerated testing in the salt spray chamber and humidity chamber. The adhesion test was conducted at room temperature according to ISO 2409.

Table 5. The results of adhesion on coatings after 96 h of testing in the salt spray chamber.

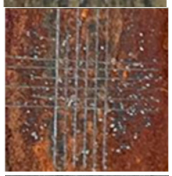
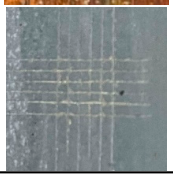
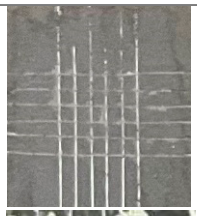
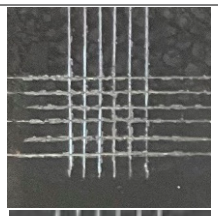
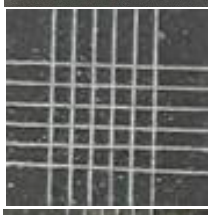
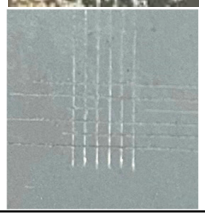
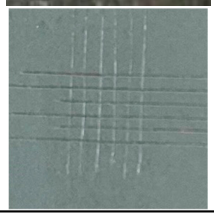
Surface Preparation	**Shot-Blasted (S)**		**Sandblasted (P)**	
Coating	**Sample Appearance**	**Grade**	**Sample Appearance**	**Grade**
SO		5		3
SE		5		1
TH		3		1
RE		2		0

Table 6. The results of adhesion on coatings after 96 h of testing in the humidity chamber.

Surface Preparation	Shot-Blasted (S)		Sandblasted (P)	
Coating	**Sample Appearance**	**Grade**	**Sample Appearance**	**Grade**
SO		1		1
SE		5		0
TH		3		0
RE		1		1

Six cuts were performed using a scalpel, spaced 1 mm apart in both the horizontal and vertical directions, forming a grid. According to the classification of test results according to ISO 2409, the samples were rated on a scale from 0 to 5. Classification 0 represents the best adhesion result; that is, the edges of the cuts are completely smooth and none of the squares of the lattice are detached [16]. Tables 6 and 7 show the results of coating adhesion testing after 96 h of exposure to accelerated testing in the salt spray and humidity chambers.

Table 7. Evaluation of degradation of coatings after 96 h of testing in the salt spray chamber.

Sample	ISO 4628-2	ISO 4628-3	ISO 4628-4	ISO 4628-8
	Blistering	**Rusting**	**Cracking**	**Corrosion around the Scribe, mm**
SO-P1	0(S0)	Ri 2	0(S0)	0.134
SO-S1	2(S3)	Ri 1	0(S0)	0.100
SE-P1	3(S2)	Ri 2	0(S0)	0.192
SE-S1	3(S3)	Ri 4	0(S0)	0.165
TH-P1	3(S2)	Ri 5	0(S0)	0.150
TH-S1	3(S2)	Ri 5	0(S0)	0.175
RE-P1	0(S0)	Ri 0	0(S0)	0
RE-S1	0(S0)	Ri 0	0(S0)	0

When examining the results, it is clear that the sandblasted samples exhibited significantly better coating adhesion after testing in the chambers compared to the shot-blasted samples. The surface had rounded small peaks after shot blasting or sharp notches after grit blasting [28]. The influence of surface preparation and roughness profile on coating

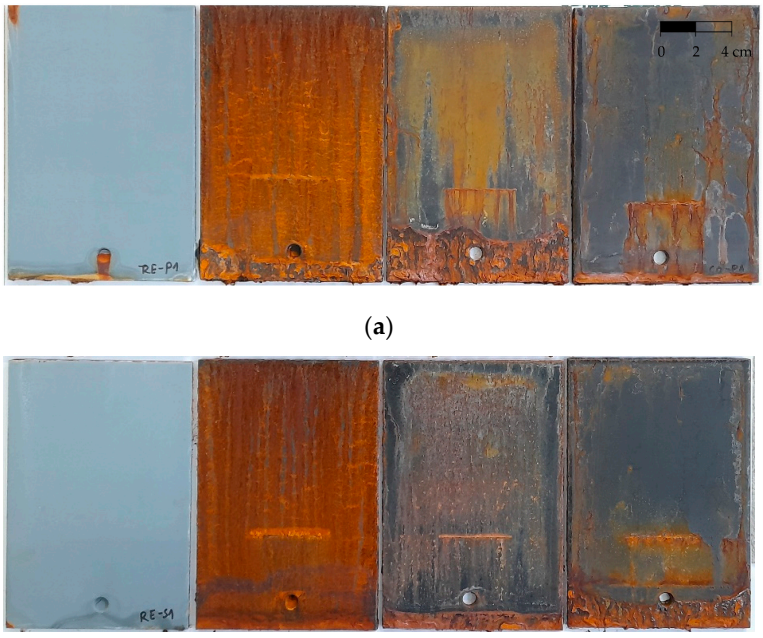
adhesion was demonstrated through these tests. Inorganic zinc ethyl silicate RE coating showed the best adhesion after testing in both chambers. Both waterborne coatings SE and TH showed poor adhesion after testing in the humidity chamber and salt spray chamber on shot-blasted samples, while SO coatings exhibited the worst adhesion after testing in the salt spray chamber on the shot-blasted samples. Generally, the samples tested in the salt spray chamber yielded the worst results. Adhesion performance is one of the most important properties of protective coatings [29]. The greater the adhesion between the coating and the substrate, the better the coating protection performance, which improves the corrosion resistance of the coating and prolongs the service life of the coating [14]. The results showed that sandblasted samples have better adhesion.

For solid coatings, adhesion strength was determined by mechanical and chemical interactions. The mechanical interactions were associated with the surface roughness of the substrate, which may lead to a mechanical interlocking between coating and substrate after coating solidification. In addition to the mechanical adhesion, chemical interactions are generally responsible for the adhesion of silicon polymers [20]. The chemical bonding between Si-polymer and substrates takes place mostly by hydrolysis and condensation reactions [20,21].

3.3. Assessment after Accelerated Testing in Salt Spray Chamber and Humidity Chamber

After 96 h of accelerated corrosion testing in the salt spray chamber (ISO 9227), all coated samples showed signs of rusting and blistering, except for the Zn-silicate coating RE, which was rust-free, according to ISO 4628. Cracking was not noticed. Corrosion around the scribe was under the maximum-allowed 1.5 mm for all samples, as according to ISO 12944-6, while the RE samples did not show any corrosion creep. The water-based modified silicone coating TH showed the worst corrosion protection in a salty environment, possibly due to low dry film thickness, from 10.3 µm to 11.3 µm. A significant extent of rust was also noticed on the SE samples, with lower dry film thickness.

The results after 96 h exposure to the salt spray chamber are shown in Figure 4 and Table 7.



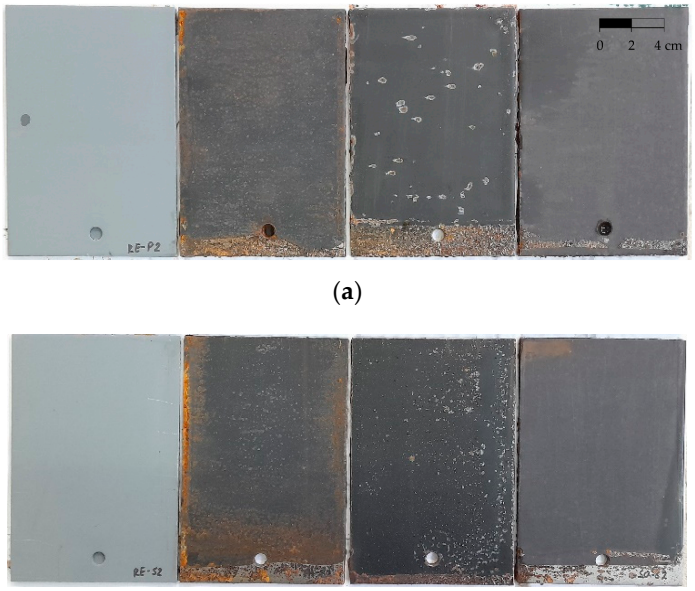
(**a**)

(**b**)

Figure 4. Coating assessment on samples RE, TH, SE, and SO (from left to right) on (**a**) sandblasted surface P and (**b**) shot-blasted surface S after 96 h exposure in the salt spray chamber, as according to ISO 9227.

After 96 h of accelerated corrosion testing in the humidity chamber (ISO 6270-2), high-temperature water-borne coatings SE and TH showed signs of rusting and blistering, whereas solvent-borne coatings SO and RE were rust-free, according to ISO 4628. Rusting and blistering were dominant on the TH-coated samples, which were protected in the lowest dry film thickness. The cracking of the tested coatings was not noticed. The edges of the samples were not considered.

The results after 96 h exposure to the humidity chamber are shown in Figure 5 and Table 8.



(**a**)

(**b**)

Figure 5. Coating assessment on samples RE, TH, SE, and SO (from left to right) on (**a**) sandblasted surface P and (**b**) shot-blasted surface S after 96 h exposure in the humidity chamber, as according to ISO 6270.

Table 8. Evaluation of degradation of coatings after 96 h of testing in the humidity chamber.

Uzorak	ISO 4628-2	ISO 4628-3	ISO 4628-4
	Blistering	Rusting	Cracking
SO-P2	0(S0)	Ri 0	0(S0)
SO-S2	0(S0)	Ri 0	0(S0)
SE-P2	0(S0)	Ri 1	0(S0)
SE-S2	3(S2)	Ri 1	0(S0)
TH-P2	4(S2)	Ri 1	0(S0)
TH-S2	3(S2)	Ri 1	0(S0)
RE-P2	0(S0)	Ri 0	0(S0)
RE-S2	0(S0)	Ri 0	0(S0)

3.4. High-Temperature Testing

To simulate the environment of a wood-burning fireplace or stove, the samples were subjected to a cyclic temperature test. They were first heated to a temperature of 450 °C for one hour, then held at that temperature for 5 h, and finally cooled to room temperature for 3 h (Figure 6). The total duration of the test was 120 h.

After the test and simulation of high-temperature cycles, the adhesion of the coatings was tested using the "Cross-cut" method, and the results obtained are shown in Table 9.

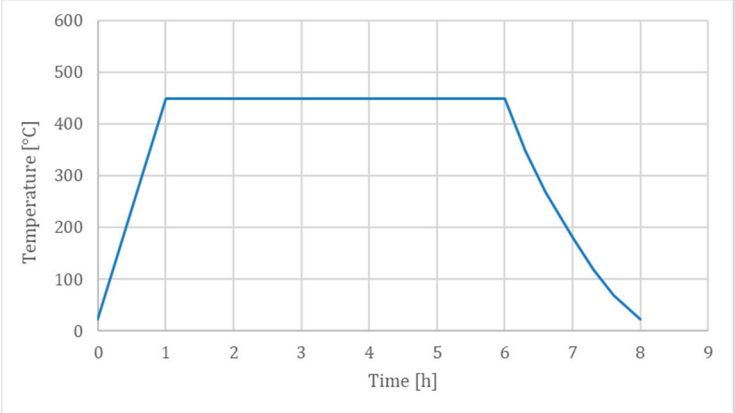
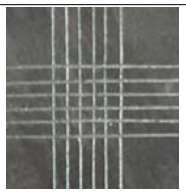
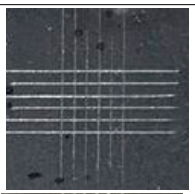
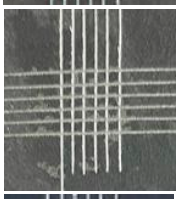
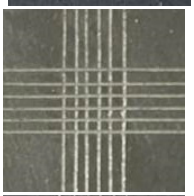
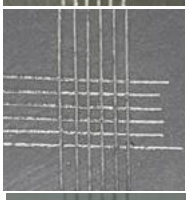
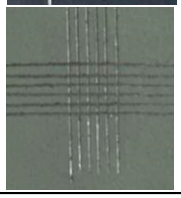
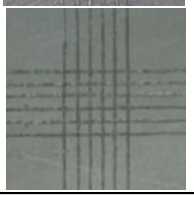


Figure 6. Test cycle time and temperature.

Table 9. The results of adhesion on coatings after high-temperature testing.

Surface Preparation	Shot-Blasted		Sandblasted	
Coating	**Sample Appearance**	**Grade**	**Sample Appearance**	**Grade**
Solvalit ATM (SO-S3, SO-P3)		0		0
Senoterm UHT 2K Hydro ATM (SE-S3, SE-P3)		2		0
Thermodur 600 Aqua ATM (TH-S3, TH-P3)		0		0
Resist 78 (RE-S3, RE-P3)		1		0

As is evident, nearly all samples exhibited excellent adhesion properties after exposure to high-temperature cycles. Also, the samples showed no defects or changes in appearance, which is extremely important as the testing environment closely resembled real conditions in a wood-burning fireplace or stove.

This property of good thermal resistance can be attributed to the chemical composition of the coating. According to [30], the major chemical compositions of the silicone-based coatings constitute Si, O, and alkali groups attached to the Si–O backbone structure. The flexible bond angle between Si and O (100–180 degrees) renders the coatings flexible, and the higher average bond energy of the Si–O bond (452 kJ/mol) makes the polymer durable at high temperatures, which is a very desirable coating property in high-temperature applications.

3.5. Electrochemical Characterization

To assess the protective performance of the coatings, the impedance modulus at the low frequency was observed. High values of absolute impedance and high coating resistance directly manifest better barrier properties [31].

Equivalent electrical circuits used to describe EIS results are shown in Figure 7a,b. Circuits consist of electrolyte resistance (R_s), coating resistance (R_c), coating capacitance (C_c), charge transfer resistance (R_{ct}), and double-layer capacitance (C_{dl}). The nonideal capacitance behaviors of the coating and double layer were described with constant phase elements Q_c and Q_{dl}, respectively [31]. Diffusion of the electrolyte to the metal substrate occurred on sample SE, so the equivalent circuit in Figure 7b was used. This circuit contained an additional element W, i.e., Warburg impedance, which describes the phenomenon of diffusion [12,13,32].

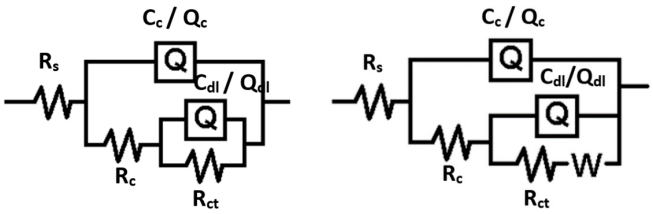


Figure 7. Equivalent electric circuit models: (**a**) electric circuit with three resistors and two capacitors, (**b**) electric circuit with three resistors, two capacitors, and Warburg impedance element W [12,13].

Nyquist and Bode plots obtained by mathematical models, according to equivalent electric circuits, together with the values of corresponding modeling errors (Chsq), are shown in Figure 8. The chi-square value (Chsq) was used to assess the goodness of fit between measured and simulated data. Better-fitting results were attained with lower chi-square values. Fitted values of equivalent circuit elements (Rs, Qc, Rc, Cdl/Qdl, and Rct) after 24 h in 3.5% NaCl are presented in Table 10.

Table 10. Fitted values of equivalent circuit elements (R_s, Q_c, R_c, C_{dl}/Q_{dl}, and R_{ct}) after 24 h in 3.5% NaCl.

Sample	R_S, (10^2 Ωcm^2)	n_c	CPE_C, (10^{-6} Fcm^2)	R_C, (10^2 Ωcm^2)	n_{dl}	C_{dl}/CPE_{dl}, (10^{-7} Fcm^2)	R_{ct}, (10^2 Ωcm^2)	W (10^{-4} Ωcm^{2}s$^{1/2}$)	DFT (μm)
SO	71.49	0.478	2.763	9.380	-	0.169	398.0	-	28.0
SE	18.07	-	0.044	56.65	0.70	151.5	69.36	3.098	29.8
TH	0.136	0.409	0.059	0.872	0.78	1239	3.328	-	30.2
RE	1.133	0.800	84.03	11.39	-	8419	13.43	-	39.1

The solvent-based coating SO exhibited the highest resistance (3.979×10^4 Ωcm^2) after exposure to the NaCl electrolyte. All coatings were applied in a similar thickness range, except for the inorganic zinc ethyl silicate RE, the thickness of which was somewhat higher. RE coating showed lower immersion resistance than expected, possibly due to porosity in the film containing a high amount of zinc dust. The protective properties of the TH water-borne coating deteriorated the most; that is, it exhibited the lowest coating resistance (3.328×10^2 Ωcm^2). This test proved that the type of coating has the greatest influence on the effectiveness of protection. Generally, coated samples with polarization resistance higher than 10^6 Ωcm^2 showed good barrier properties [31]. All tested coatings in this study showed lower resistance, probably due to their chemical composition and purpose for indoor protection when applied in low dry film thickness. Due to the flexible Si–O bond angle, the disadvantage of using silicone coatings is related to the high permeation rate for atmospheric constituents such as moisture, oxygen, and other gaseous elements [30], which may result in weaker corrosion protection properties.

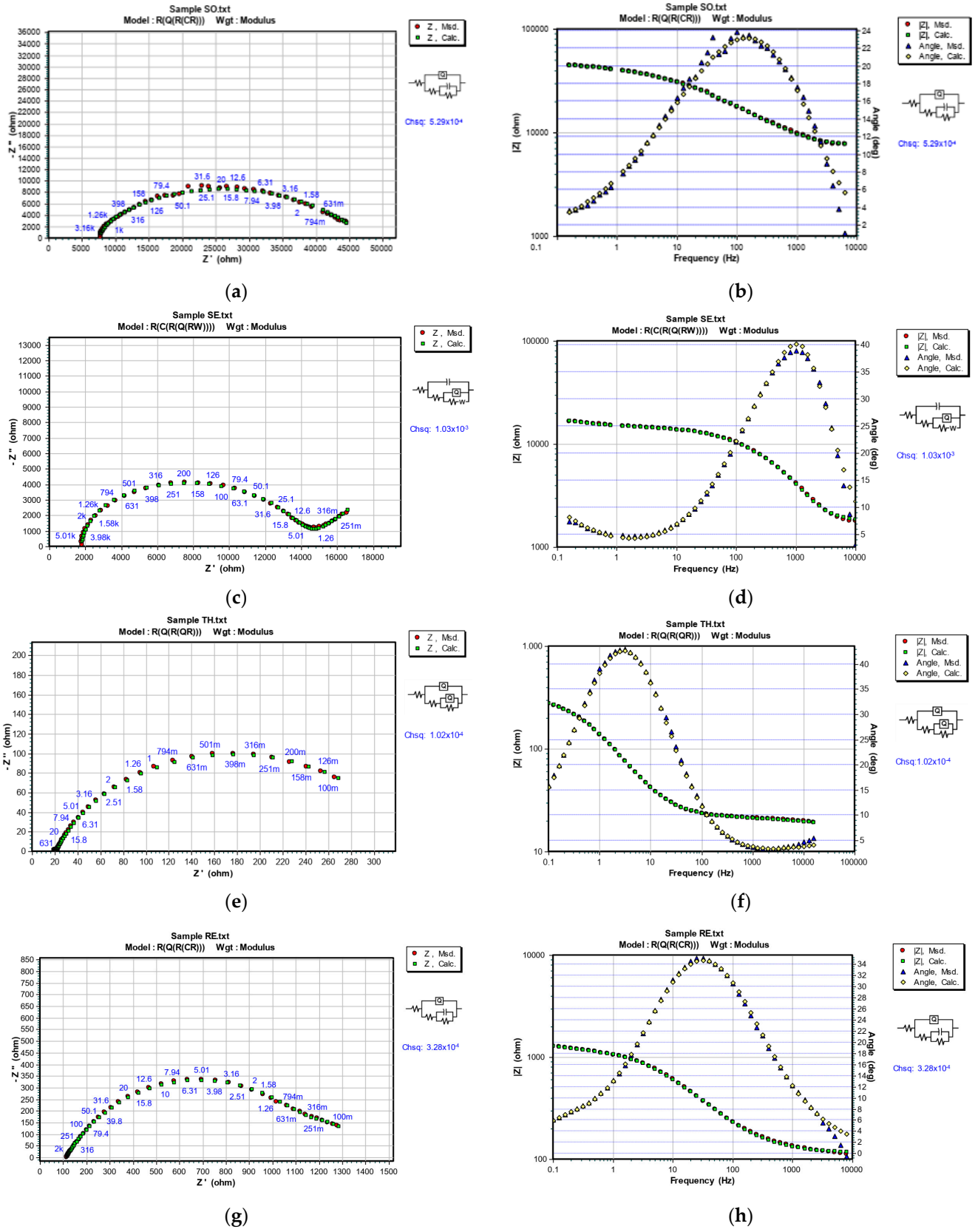


Figure 8. Nyquist and Bode plots for each sample after 24 h in 3.5% NaCl solution. Nyquist diagrams are represented in (**a**) SO, (**c**) SE, (**e**) TH, and (**g**) RE, while Bode and phase-angle plots are shown in (**b**) SO, (**d**) SE, (**f**) TH, and (**h**) RE.

3.6. Differential Scanning Calorimetry (DSC)

To determine the phase transitions of silicone-based coatings, a differential scanning calorimetry was used. DSC thermograms for the second heating cycle are shown in Figure 9. Sample RE achieves the highest glass transition temperature among the samples, reaching 100.86 °C, potentially indicating superior thermal stability compared to other samples. Sample SE closely approaches the highest glass transition temperature, measuring 88.86 °C. The lowest temperatures are observed in samples SO and TH, presented in Figure 9a,b, at 48.59 °C and 26.72 °C, respectively. These temperatures closely correspond to the glass transition values for silicone acrylic coatings as detailed in [33].

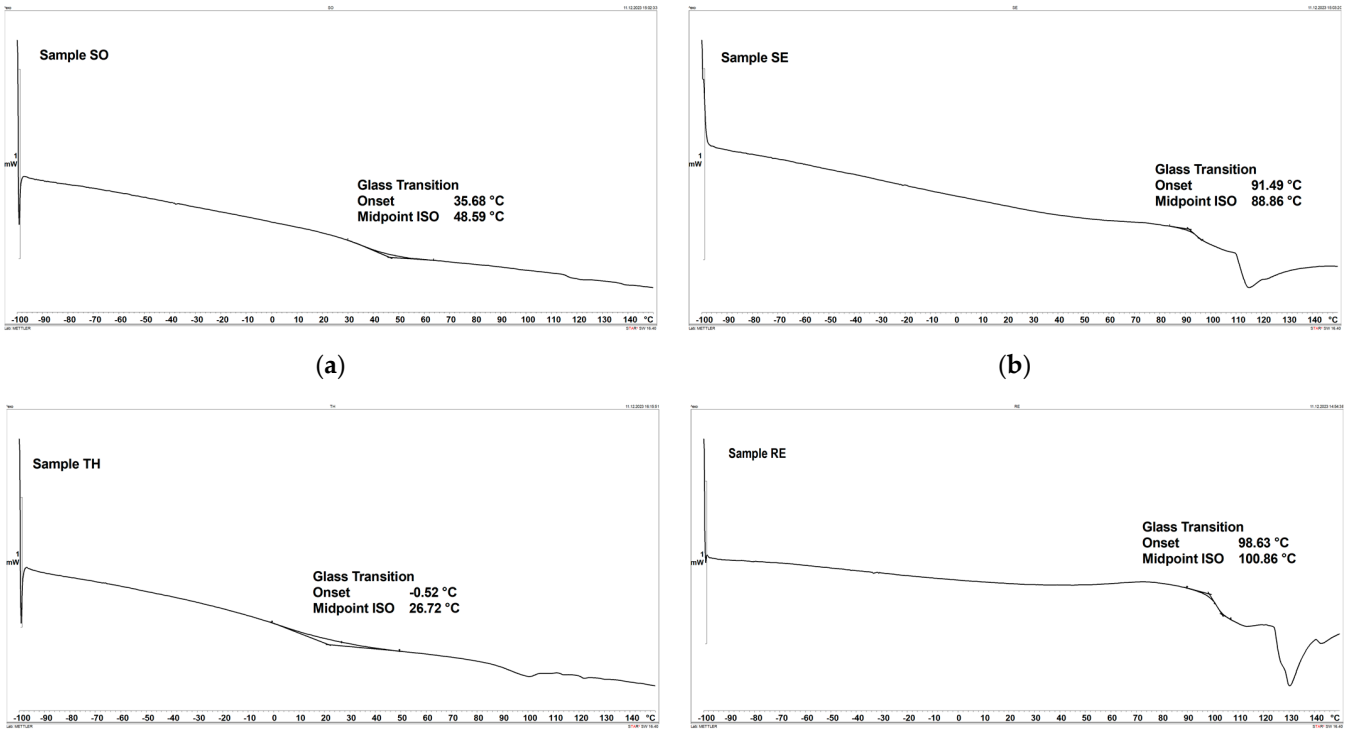


Figure 9. DSC thermograms for high-temperature coatings (**a**) SO, (**b**) SE, (**c**) TH, and (**d**) RE.

4. Conclusions

High-temperature coatings are widely used for protecting metal objects exposed to high temperatures, such as furnaces and stoves. In addition to requiring good corrosion and cyclic temperature resistance, they need to have a visually appealing surface, which can be challenging to maintain if the coatings are exposed to a salty atmosphere, as shown by this research.

The following conclusions can be drawn from this study:

- The sandblasted samples exhibited significantly better coating adhesion after testing in the salt spray and humidity chambers compared to the shot-blasted samples. After the salt spray chamber test, with the SO and SE samples, there was a complete detachment (classification 5 according to ISO 2409) of the coatings applied on the shot-blasted samples.
- The best-performing coating in the accelerated chamber testing was inorganic zinc ethyl silicate, which not only exhibited excellent properties but also maintained a decent external appearance from an esthetic perspective.
- Coating hardness was equal for all tested coatings, probably due to the great influence of the steel substrate.

- The EIS results show that solvent-based coatings have better barrier properties than water-based coatings. The solvent-based coating SO exhibited the highest resistance, which is 10^1 Ωcm^2 orders higher than water-based coating SE and 10^2 Ωcm^2 orders higher than water-based coating TH.
- The DSC results show that sample RE achieves the highest glass transition temperature, measuring 100.86 °C, while sample TH exhibits the lowest temperature, measuring 26.72 °C.
- The properties and appearances of the coatings are more favorable in humid conditions and high-temperature environments, which align with the real-world application conditions for coating protection of wood-burning stoves.

Author Contributions: B.Š. and I.S. performed the experiments and wrote the paper. I.S. designed the experiments and analyzed the data. V.A. and M.K. revised and edited the paper. M.O. performed and analyzed DSC. All authors have read and agreed to the published version of the manuscript.

Funding: This research was funded by the European Regional Development Fund, grant number KK 01.2.1.02.0226.

Institutional Review Board Statement: Not applicable.

Informed Consent Statement: Not applicable.

Data Availability Statement: The data presented in this study are available on request from the corresponding author.

Acknowledgments: This study is based on the project "Development of a Highly Energy Efficient Solid Fuel Heating System from Renewable Energy Sources Using Innovative Technological Processes", which is co-financed within the Operational Programme Competitiveness and Cohesion from the European Regional Development Fund under reference number KK. 01.2.1.02.0226.

Conflicts of Interest: The authors declare no conflict of interest.

References

1. Bose, S. *High Temperature Coatings*; Butterworth-Heinemann: Oxford, UK, 2017.
2. Lai, G.Y. High-Temperature Corrosion and Materials Applications. In *High-Temperature Corrosion and Materials Applications*; ASM International: Detroit, MI, USA, 2007; Volume 2.
3. Zielecka, M.; Rabajczyk, A.; Cygańczuk, K.; Pastuszka, Ł.; Jurecki, L. Silicone Resin-Based Intumescent Paints. *Materials* **2020**, *13*, 4785. [CrossRef] [PubMed]
4. Mévrel, R. State of the art on high-temperature corrosion-resistant coatings. *Mater. Sci. Eng. A* **1989**, *120*, 13–24. [CrossRef]
5. Bellamy, G.T.; DiDomizio, M.J.; Patel, M.K.; McKinnon, M.B. Characterization of high-temperature paints for infrared thermography in fire research. *Fire Saf. J.* **2023**, *137*, 103775. [CrossRef]
6. Chew, K.W.; Yahaya, A.H.; Arof, A.K. Studies on the properties of silicone resin films on mild steel. *Pigment. Resin Technol.* **2000**, *29*, 364–368. [CrossRef]
7. Mathivanan, L.; Selvaraj, M.; Azim, S.S.; Balakrishnan, K. Evaluation of heat resistant properties of silicone-based coatings by SEM and a.c. Impedance techniques. *Prog. Org. Coat.* **1996**, *28*, 113–116. [CrossRef]
8. Ramakrishnan, M. Epoxy High Temperature Coatings and Considerations. In Proceedings of the Corrosion 2017, New Orleans, LO, USA, 26–30 March 2017; NACE International: Houston, TX, USA, 2017; p. 9430.
9. Mathivanan, L.; Arof, A.K. The degradation of silicone coatings in high-temperature atmospheres. *Anti-Corros. Methods Mater.* **1998**, *45*, 403–412. [CrossRef]
10. Xu, J.; Long, J.; Zhang, R.; Du, J.; Guan, S.; Wang, Y.; Huang, L.; Wei, H.; Liu, L.; Huang, Y. Greatly improving thermal stability of silicone resins by modification with POSS. *Polym. Degrad. Stab.* **2020**, *174*, 109082. [CrossRef]
11. Gao, H.; Xiong, Y.; Zhang, K.; Cao, S.; Hu, M.; Li, Y.; Zhang, P.; Liu, X. Molecular Dynamics Simulation of Interface Properties between Water-Based Inorganic Zinc Silicate Coating Modified by Organosilicone and Iron Substrate. *J. Renew. Mater.* **2023**, *11*, 1715–1729. [CrossRef]
12. Alsamuraee, A.M.A.; Jaafer, I.H.; Ameen, A.H.; Abdullah, Q.A. Electrochemical impedance spectroscopic evaluation of cor-rosion protection properties of polyurethane/polyvinyl chloride blend coating on steel. *Am. J. Sci. Res.* **2011**, *2*, 761–768. [CrossRef]
13. Stojanović, I.; Logar, M.; Fatović, I.; Alar, V.; Rakela-Ristevski, D. Experimental Study of Atmospherically and Infrared-Dried Industrial Topcoats. *Coatings* **2023**, *13*, 1343. [CrossRef]
14. Chen, J.; Liu, J.; Wang, H.; Li, B.; Hu, Q.; Shao, T.; Yang, R.; Wang, B.; Wan, Q.; Li, Z.; et al. Experimental Study on Neutral Salt Spray Accelerated Corrosion of Metal Protective Coatings for Power-Transmission and Transformation Equipment. *Coatings* **2023**, *13*, 480. [CrossRef]

15. Tsai, P.-Y.; Chen, T.-E.; Lee, Y.-L. Development and Characterization of Anticorrosion and Antifriction Properties for High Performance Polyurethane/Graphene Composite Coatings. *Coatings* **2018**, *8*, 250. [CrossRef]
16. *ISO 2409*; Paints and Varnishes—Cross-Cut Test. International Organization for Standardization: Geneva, Switzerland, 2020.
17. Aračić, S.; Krumes, S.; Matičević, T. Research into the possibility of using the new generation paint systems for the anticorrosion protection of steel structures. *Tech. Gaz.* **2009**, *16*, 75–79.
18. *ISO 6270*; Paints and Varnishes—Determination of Resistance to Humidity—Part 1: Condensation (Single-Sided Exposure). International Organization for Standardization: Geneva, Switzerland, 2017.
19. *ISO 4628*; Paints and Varnishes—Evaluation of Degradation of Coatings—Designation of Quantity and Size of Defects, and of Intensity of Uniform Changes in Appearance—Part 1: General Introduction and Designation System. International Organization for Standardization: Geneva, Switzerland, 2016.
20. Barroso, G.; Li, Q.; Bordia, R.K.; Motz, G. Polymeric and ceramic silicon-based coatings—A review. *J. Mater. Chem. A* **2019**, *7*, 1936–1963. [CrossRef]
21. Indumathy, B.; Sathiyanathan, P.; Prasad, G.; Reza, M.S.; Prabu, A.A.; Kim, H. A Comprehensive Review on Processing, Development and Applications of Organofunctional Silanes and Silane-Based Hyperbranched Polymers. *Polymers* **2023**, *15*, 2517. [CrossRef]
22. Hoang, N.; Khoa, T.A.; Nhung, L.T.; Phuong, P.M.; Binh, T.D.; Hang, T.T.X.; Chi, N.V.; Nguyen, T.-D. Flake ZnAl Alloy as an Effective Pigment in Silicate Coatings for the Corrosion Protection of Steel. *Coatings* **2022**, *12*, 1046. [CrossRef]
23. *ISO 2808*; Paints and Varnishes—Determination of Film Thickness. International Organization for Standardization: Geneva, Switzerland, 2019.
24. *ISO 9227*; Corrosion Tests in Artificial Atmospheres—Salt Spray Tests. International Organization for Standardization: Geneva, Switzerland, 2022.
25. *ISO 12944-6*; Paints and Varnishes—Corrosion Protection of Steel Structures by Protective Coating Systems—Part 6: Laboratory Performance Test Methods. International Organization for Standardization: Geneva, Switzerland, 2018.
26. *ISO 8501-1*; Preparation of Steel Substrates before Application of Paints and Related Products—Visual Assessment of Surface Cleanliness—Part 1: Rust Grades and Preparation Grades of Uncoated Steel Substrates and of Steel Substrates after Overall Removal of Previous Coatings. International Organization for Standardization: Geneva, Switzerland, 2007.
27. Kralj, M.; Pavković, K.; Stojanović, I.; Anđal, J. Adhesion and anticorrosive properties of DTM coating as related to primer coating. *Građevinar* **2018**, *71*, 401–408. [CrossRef]
28. Draganovská, D.; Brezinová, J.; Guzanová, A. Surface Characterization after Blasting. In *Tribology of Machine Elements*; Pintaude, G., Cousseau, T., Rudawska, A., Eds.; IntechOpen: London, UK, 2022. [CrossRef]
29. Lyon, S.B.; Bingham, R.; Mills, D.J. Advances in corrosion protection by organic coatings: What we know and what we would like to know. *Prog. Org. Coat.* **2017**, *102*, 2–7. [CrossRef]
30. Ambat, R.; Piotrowska, K. Preventive measures for corrosion in electronics: Intrinsic and extrinsic strategies. In *Humidity and Electronics*; Ambat, R., Piotrowska, K., Eds.; Woodhead Publishing: Sawston, UK, 2022; pp. 285–337. [CrossRef]
31. Stojanović, I.; Cindrić, I.; Turkalj, L.; Kurtela, M.; Rakela-Ristevski, D. Durability and Corrosion Properties of Waterborne Coating Systems on Mild Steel Dried under Atmospheric Conditions and by Infrared Radiation. *Materials* **2022**, *15*, 8001. [CrossRef]
32. Šoić, I.; Martinez, S.; Dubravić, M. Gel-Electrolyte EIS setup used for probing of IR Dried/Cured industrial coatings. *Prog. Org. Coat.* **2019**, *137*, 105331. [CrossRef]
33. Park, H.S.; Kim, S.R.; Park, H.J.; Kwak, C.; Hahm, H.S.; Kim, S.K. Preparation and Characterization Of Weather Resistant Silicone/Acrylic Resin Coatings. *J. Coat. Technol.* **2003**, *75*, 55–64. [CrossRef]

Disclaimer/Publisher's Note: The statements, opinions and data contained in all publications are solely those of the individual author(s) and contributor(s) and not of MDPI and/or the editor(s). MDPI and/or the editor(s) disclaim responsibility for any injury to people or property resulting from any ideas, methods, instructions or products referred to in the content.